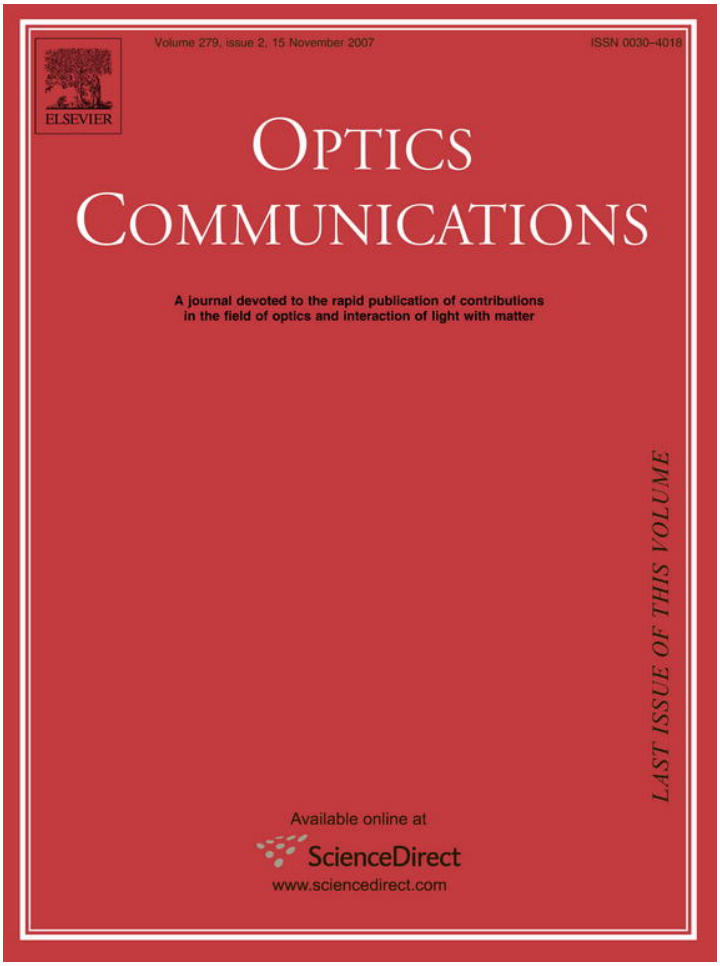

Available online at www.sciencedirect.com
ScienceDirect
Optics Communications 279 (2007) 370–376
OPTICS COMMUNICATIONS
www.elsevier.com/locate/optcom

Full-vectorial analysis of optical vortex propagation in anisotropic cubic-quintic non-linear optical medium

Ben-Hur V. Borges [a,*], Amilcar C. César [a], Licinius D.S. Alcantara [b]

[a] University of São Paulo-USP, Electrical Engineering Department, Av. Trabalhador São-Carlense, 400, 13566-590 São Carlos, SP, Brazil
[b] Federal University of Para-UFPA, Electrical Engineering and Computing Department, Guama Campus, Rua Augusto Correa, 01, CEP 66075-900 Belém, PA, Brazil

Received 28 March 2007; received in revised form 10 July 2007; accepted 13 July 2007

Abstract

This paper presents for the first time a full-vectorial analysis of optical vortex propagation in anisotropic cubic-quintic (CQ) non-linear medium. The purpose is to investigate the energy transfer mechanism and stability between orthogonal field components and how they are affected by the presence of material anisotropy in CQ materials. The numerical simulations were carried out via a three-dimensional finite difference based beam propagation method (3D-FD-BPM) which is capable of handling variations in any of the permittivity tensor components. Therefore, in this work we allowed all tensor components to vary independently and simulate vortex propagation for distances several times longer than the diffraction length. We expect that this work can provide new and important information regarding the behavior of these objects that may become valuable for the design of new photonic devices.

Keywords: Optical vortex; Cubic-quintic; Anisotropy; Stability; Non-linear optics; Soliton propagation

1. Introduction

The study of phase singularities in wave propagation has attracted a great deal of attention of the scientific community since they were first reported in 1974 by Nye and Berry [1]. At the singularity point the phase of the wave is not defined and its amplitude vanishes. In light waves, the phase singularity gives rise to a fascinating object called optical vortex, experimentally investigated in non-linear optics in the pioneering work by Swartzlander et al. [2]. The first theoretical study on this subject, by its turn, is due to Snyder et al. [3]. The familiar doughnut (ring) shape of these objects is a consequence of its internal vorticity which creates a dark center inside it [4]. Readers interested in a more detailed description of optical vortex characteristics are referred to [5,6] and references therein.

One major issue in bright vortex soliton propagation is its instability. It is well known that this object tends to become unstable against azimuthal perturbations [4,7]. One way of preventing this instability from occurring is through the competition between a focusing $\chi^{(2)}$ non-linearity and a self-defocusing $\chi^{(3)}$ non-linearity, as suggested by [8]. Another approach consists in adopting an optical model based on the competition between cubic and quintic non-linearities (it is noteworthy mentioning that the first stable vortex soliton was observed for this model [9–11]). Stability issues concerning isotropic cubic-quintic (CQ) models have been successfully addressed in [12,13], and was extended even further by Mihalache et al. [14] with the inclusion of self-phase modulation, cross-phase modulation, and four-wave mixing effects in the cubic part of the model. Additionally, by assuming CQ materials as isotropic allows one to obtain vortex solitons with spin values as high as five [15]. It should be mentioned at this point that stable two-dimensional vortex solitons can also be formed in dissipative systems described by a complex CQ

* Corresponding author. Tel.: +55 16 3373 8132; fax: +55 16 3373 9372.
E-mail address: benhur@sel.eesc.usp.br (Ben-Hur V. Borges).

0030-4018/$ - see front matter © 2007 Elsevier B.V. All rights reserved.
doi:10.1016/j.optcom.2007.07.013

Ginzburg–Landau equation according to Crasovan et al. [16], where it is shown that both non-spinning and spiral solitons are remarkably stable against azimuthal perturbations. Another issue of growing interest for both theoretical and experimental studies is the possibility of forming stable three-dimensional (3D) spatiotemporal vortex solitons in both conservative and dissipative non-linear optical media. It has been demonstrated by Mihalache et al. [17–19] that 3D vortex tori can be stable under certain conditions in media with competing optical non-linearities of the quadratic-cubic or cubic-quintic types. In any case, all CQ models currently available in the literature assume the CQ non-linear media as isotropic.

The effect of material anisotropy in vortex propagation has been investigated quite successfully for photorefractive materials (which are known for producing unstable vortex propagation) [5,11,20]. Therefore, being able to simulate either isotropic or anisotropic CQ non-linear media may prove to be quite useful for a complete understanding of the propagation dynamics of this fascinating non-linear object. Since optical vortices can be utilized to induce waveguide channels in a bulk non-linear medium, an interesting application would be the possibility of inducing stable, directionable, and non-diffractive waveguides in order to allow the guidance of other beams in a steerable manner [21]. In addition to including anisotropy, one should also include the vectorial properties of light propagation, since it might play an important role in the design of future polarization sensitive devices.

In this paper, we demonstrate, for the first time to our knowledge, a full-vectorial approach for the simulation of optical vortex propagation in anisotropic CQ non-linear media. This model, originally introduced by Alcantara et al. [22] to simulate the propagation of light condensates in these materials, is a finite difference beam propagation method (FD-BPM) that solves the full-vectorial Helmholtz equation. We consider different variations of the anisotropy for all three axis of the permittivity tensor so that the stability issue for this particular medium can be addressed.

This paper is organized as follows. In Section 2 we introduce the full-vectorial Helmholtz equation for the modeling of anisotropic CQ non-linear media. In Section 3 we describe the optical properties of this medium and investigate how small variations of the permittivity tensor elements affect the stability of vortex propagation. Also discussed in this section is how the anisotropy, particularly along the z-axis, affects the energy distribution between orthogonal field components. Finally, Section 4 presents some concluding remarks for this paper.

2. Model

The formalism employed to simulate these objects is the full-vectorial Helmholtz equation for the electric field $\overline{E}(x,y,z)$, which reads [22]

$$k_0^2\overline{\overline{\varepsilon}}\overline{\mathrm{E}} + \nabla^2\overline{E} = \nabla(\nabla\cdot\overline{E}), \tag{1}$$

where $k_0 = 2\pi/\lambda_0$ is the propagation constant in vacuum. The dielectric relative permittivity tensor is given by

$$\overline{\overline{\varepsilon}} = \begin{pmatrix} \varepsilon_{xx} & 0 & 0 \\ 0 & \varepsilon_{yy} & 0 \\ 0 & 0 & \varepsilon_{zz} \end{pmatrix} = \varepsilon_0 \begin{pmatrix} n_{xx}^2 & 0 & 0 \\ 0 & n_{yy}^2 & 0 \\ 0 & 0 & n_{zz}^2 \end{pmatrix}. \tag{2}$$

where the double overbar denotes that the permittivity is being considered in a tensorial form. Expanding (1) for the transversal field components, results

$$k_0^2\varepsilon_{xx}E_x + \frac{\partial^2 E_x}{\partial y^2} + \frac{\partial^2 E_x}{\partial z^2} = \frac{\partial}{\partial x}\left(\frac{\partial E_y}{\partial y} + \frac{\partial E_z}{\partial z}\right), \tag{3}$$

$$k_0^2\varepsilon_{yy}E_y + \frac{\partial^2 E_y}{\partial x^2} + \frac{\partial^2 E_y}{\partial z^2} = \frac{\partial}{\partial y}\left(\frac{\partial E_x}{\partial x} + \frac{\partial E_z}{\partial z}\right). \tag{4}$$

As one can observe, Eqs. (3) and (4) clearly show the coupling between all three electric field components. Solving Eqs. (3) and (4) directly is quite a challenging task, but these equations can be recast in terms of transverse field components only (E_x and E_y) in a lengthy, but straightforward manner. In order to do so, first one needs to expand the Gauss' law ($\nabla\cdot(\overline{\overline{\varepsilon}}\overline{E}) = 0$) for the E_z component and to assume slow variation of ε_{zz} along the propagation axis, so that longitudinal derivatives related to this quantity can be neglected. As a result, the following equation for the longitudinal component can be obtained.

$$\frac{\partial E_z}{\partial z} = -\frac{1}{\varepsilon_{zz}}\left[\frac{\partial}{\partial x}(\varepsilon_{xx}E_x) + \frac{\partial}{\partial y}(\varepsilon_{yy}E_y)\right]. \tag{5}$$

Next, by substituting (5) into (3)-(4) one ends up with a new coupled system involving E_x and E_y, as expected. Once the new coupled system has been obtained, the following step consists in applying the slowly varying envelope approximation which consists in redefining the field amplitude as

$$\overline{E}(x,y,z) = \overline{\Psi}(x,y,z)\exp(-\mathrm{j}\kappa z),$$

where $\kappa = k_0 n_0$ and n_0 is the reference refractive index. This field amplitude is then substituted back into the new coupled system, and the resulting equations are reduced to a set of coupled parabolic equations via paraxial approximation, i.e., $|\partial^2\overline{\Psi}/\partial z^2| \ll 2\kappa|\partial\overline{\Psi}/\partial z|$. As a result, one finally obtains

$$k_0^2(\varepsilon_{xx} - n_0^2)\Psi_x + F_x\Psi_x + D_y\Psi_x - 2\mathrm{j}\kappa\frac{\partial\Psi_x}{\partial z} = P_{xy}\Psi_y, \tag{6}$$

$$k_0^2(\varepsilon_{yy} - n_0^2)\Psi_y + D_x\Psi_y + F_y\Psi_y - 2\mathrm{j}\kappa\frac{\partial\Psi_y}{\partial z} = P_{yx}\Psi_x, \tag{7}$$

where

$$F_x = \frac{\partial}{\partial x}\left[\frac{1}{\varepsilon_{zz}}\frac{\partial}{\partial x}(\varepsilon_{xx})\right],$$
$$F_y = \frac{\partial}{\partial y}\left[\frac{1}{\varepsilon_{zz}}\frac{\partial}{\partial y}(\varepsilon_{yy})\right],$$
$$D_x = \frac{\partial^2}{\partial x^2}, \quad D_y = \frac{\partial^2}{\partial y^2},$$
$$P_{xy} = \frac{\partial^2}{\partial x \partial y} - \frac{\partial}{\partial x}\left[\frac{1}{\varepsilon_{zz}}\frac{\partial}{\partial y}(\varepsilon_{yy})\right],$$
$$P_{yx} = \frac{\partial^2}{\partial y \partial x} - \frac{\partial}{\partial y}\left[\frac{1}{\varepsilon_{zz}}\frac{\partial}{\partial x}(\varepsilon_{xx})\right].$$

The electric permittivity tensor components in the CQ non-linear media are assumed to have the following electric field dependence (Kerr-type medium with saturation):

$$\varepsilon_{uu} = \varepsilon_{uu}^{L} + \alpha_2|\Psi|^2 - \alpha_4|\Psi|^4,$$

where uu stands for xx, yy or zz, superscript L indicates the linear relative permittivity, and $|\Psi|$ is defined as

$$|\Psi| = \sqrt{|\Psi_x|^2 + |\Psi_y|^2 + |\Psi_z|^2}, \tag{8}$$

where Ψ_z is obtained from Gauss' law. The finite difference discretization of (6) and (7) along the z-axis follows that of [22], and will be omitted here. A transparent boundary condition is also implemented at the edges of the computational domain in order to suppress unwanted reflections.

3. Numerical results and discussions

In cubic-quintic non-linear materials the refractive index dependence with respect to field intensity is well characterized by a cubic focusing term (owed to optical Kerr effect) and a quintic defocusing term. The important characteristic of these competing non-linearity effects is the possibility of producing stable beam propagation for a given optical intensity. Promising candidates for this application are chalcogenide glasses, as well pointed out by [23,24].

The model structure investigated in this work is a bulk non-linear medium similar to the one described in [22,23], but we have changed the refractive index to $n_L = 2.5$ in order to adequate it to some of the available data for chalcogenide glasses [25,26]. The focusing and defocusing non-linear coefficients are $\alpha_2 = 1.89 \times 10^{-18}\ \mathrm{m^2/V^2}$ and $\alpha_4 = 1.64 \times 10^{-34}\ \mathrm{m^4/V^4}$, respectively. The simulation parameters adopted are: wavelength $\lambda = 1.064\ \mu\mathrm{m}$, transverse step size $\delta_x = \delta_y = 0.5\ \mu\mathrm{m}$, longitudinal step size $\delta_z = 0.2\ \mu\mathrm{m}$, and number of discretization cells $N_x = N_y = 300$. The input field is assumed as a Gaussian distribution illuminating an appropriate phase mask [23]:

$$\psi = A\exp\left[-\frac{(x^2+y^2)}{2\omega_0^2}\right]e^{iq\theta},$$

where $A = 107.381116 \times 10^6\ \mathrm{V/m}$, $\omega_0 = 11\ \mu\mathrm{m}$, q is the topological charge, and $\theta = \tan^{-1}(y/x)$. The amplitude A is chosen, so that the contribution of the focusing and defocusing non-linear coefficients to the refractive index cancels each other ($A = \sqrt{\alpha_2/\alpha_4}$), which corresponds to a stable vortex propagation in a linear case. The excitation is applied to the E_x component, while $E_y = E_z = 0$ at $z = 0$. The topological charge assumed in all simulations is $q = 1$.

The simulations indicate that the vortex propagation is quite stable if the anisotropy occurs only in the x or y component of the relative permittivity tensor, $\bar{\bar{\varepsilon}}$. In fact, we have simulated long propagation distances for both cases, allowing the tensor components ε_{xx} and ε_{yy} to vary independently from 6.25 ($n = 2.5$) to 6.890625 ($n = 2.625$), which represents a variation of up to 5% in the corresponding refractive index. Therefore, for every variation of the tensor components a new simulation run was carried out, with the tensor values kept constants, even in the longitudinal direction. It is worth mentioning that the vortex ring for the excited component (E_x in these cases) is not perturbed by the anisotropy introduced in the material even when long propagation distances are required. This behavior prevents it from getting unstable, and constitutes an important parameter for the designing of optical devices. As an example, the intensity isosurface for E_x and the intensity versus propagation distance for E_x and E_y are shown in Fig. 1a and b, respectively. The intensities are obtained by solving $I_u(z) = \int\int |E_u(x,y,z)|^2\,dx\,dy$, with $u = x$ or y. It is assumed in here a strong anisotropy along the x-axis of the tensor, that is, $n_{xx} = 2.5 + \Delta$, with $\Delta = 0.125$, and $n_{yy} = n_{zz} = 2.5$. These parameters do not change during the simulation. The propagation distance is 100 mm. It can be observed that after an initial accommodation the field intensity no longer changes as it propagates, i.e., it remains confined in the induced channel created by the vortex ring. The results also indicate that there is no significant transfer of energy between the transversal field components. In fact, in all simulations where either n_{xx} or n_{yy} were allowed to vary, the intensity ratio $I = |E_y/E_x|^2$ did not show any significant variation, and plateaus at a level approximately eight orders of magnitude smaller than that for the x component. The result in Fig. 1a also shows that the vortex experiences an off-center drift as it propagates (this behavior was observed either for the isotropic and anisotropic case). Off-center drifts have been demonstrated for dark vortex solitons as a result of background gradients of phase [27,28]. In the present case, part of the energy is also dissipated during propagation, leading to a breaking of the cylindrical symmetry with respect to the vortex axis [29], and consequently to an off-center drift. It is worth mentioning that the excitation field adopted in all simulations immediately develops a singularity in its center since the phase is not defined in this location. Consequently, a strong disturbance is verified in the field in the early stage of propagation ($z < 0.1$ mm). After this distance, the field distribution assumes its familiar doughnut shape helped by the combined effects of focusing and defocusing non-linearities. This behavior is not seen in the isosurfaces due to the resolution adopted in generating these figures.

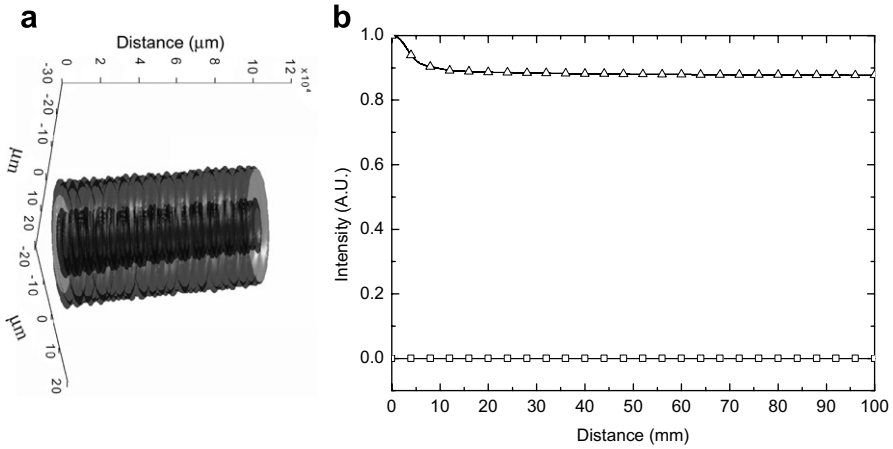

Fig. 1. Vortex propagation for an anisotropic CQ non-linear material with $n_{yy} = n_{zz} = 2.5$, and $n_{xx} = 2.5 + \Delta$, with $\Delta = 0.125$. (a) Intensity isosurface for the E_x component, showing a stable vortex propagation and (b) field intensity versus propagation distance for the transverse components E_x (triangles) and E_y (squares). The propagation distance is $z = 100$ mm.

The smooth behavior described above is no longer observed when the anisotropy is introduced in the z component of the permittivity tensor, i.e., ε_{zz}. As will become clear next, the vortex soliton becomes unstable for any value of anisotropy for this particular tensor component. In order to demonstrate the drastic changes in the vortex stability, we increased the propagation distance to 300 mm so that the dynamics of energy transfer between the transversal field components can be better visualized. In the present case, the tensor components $\varepsilon_{xx} = \varepsilon_{yy} = 6.25$ ($n_{xx} = n_{yy} = 2.5$), while ε_{zz} is allowed to vary from 6.25 ($n_z = 2.5$) up to 6.890625 ($n_{zz} = 2.625$, corresponding to a refractive index variation of 5%). Observe that a new simulation run is carried out for every value of ε_{zz}, with all tensor elements kept fixed.

One important aspect, common to all cases where only n_{zz} varies, is the splitting of the vortex ring. Splitting of the vortex can in fact be observed for different model problems where instabilities play a significant role, as described in [30]. In the present case, this phenomenon occurs even for low anisotropy values, affecting severely the stability of these objects. As an example, consider the case where $n_{zz} = 2.5 + \Delta$, where $\Delta = 0.05$ (2% refractive index variation). Isosurfaces plots illustrating the intensity evolution for the transversal field components are shown in Fig. 2 for a propagation distance of 100 mm. The splitting of the vortex ring can clearly be seen at $z \approx 40$ mm and, as it starts, the energy exchange between the transversal field components increases rapidly, with an oscillatory behavior as one would expect. The splitting is caused by a symmetry breaking due to the anisotropy. It is worthy mentioning that the symmetry breaking begins with significant intensity oscillations along the top of the ring which increase and dramatically deform the ring as the propagation progresses. In addition, there is also a dramatic energy exchange between field components (E_x and E_y), each one contributing differently to the local refractive index along the propagation, favoring modulational instabilities.

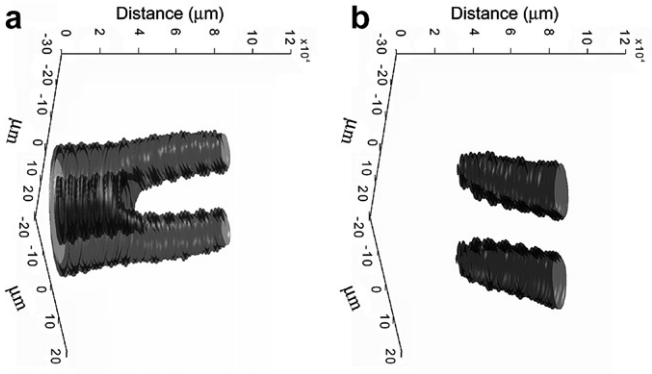

Fig. 2. Isosurface of the field intensity evolution in an anisotropic CQ nonlinear material with $n_{xx} = n_{yy} = 2.5$ and $n_{zz} = 2.5 + \Delta$, where $\Delta = 0.05$. (a) E_x component, and (b) E_y component (this isosurface was rotated to help visualization).

Once the splitting occurs, the resulting solution forms a bound composite state that stabilizes each other for a certain distance, forming a dipole-mode soliton [31]. In fact, it remains stationary for tens of diffraction lengths, in the same fashion as described in [31–33]. During the dipole-mode soliton formation the intensity of both field components becomes quite significant by virtue of anisotropy, and strongly interacts with each other (this will become clear later on when we discuss the energy exchange mechanism between field components). Observe that the intensity maxima of each field component occur at the position of the minima of the other due field orthogonality. Consequently, their individual contribution to the local refractive index causes a trapping of the dipole-mode beam as seem by each component, preventing it from flying off tangentially. It should also be pointed out that both components present a consistent oscillatory behavior during this stage, very similar to the one reported in [32]. Eventually, the symmetry breaking introduced by the anisotropy gives rise to numerical noise that causes the dipole-mode soliton to break apart and repel each other. This process starts at

$z \approx 140$ mm (observe the E_y component). The breaking-up of the structure becomes more dramatic at $z \approx 280$ mm, ending up in two solitons being ejected tangentially. This process can be observed in Fig. 3, which shows the vortex evolution at different positions along the propagation direction.

By increasing the anisotropy even further, i.e., $n_{zz} = 2.5 + \Delta$, where $\Delta = 0.125$, the energy exchange, and consequently the instability arising from symmetry breaking, increases more drastically. As a result, the splitting of the vortex ring starts much earlier than the previous case (at $z \approx 5$ mm, less than a diffraction length). Even for this extreme situation, a bound state is also formed after the splitting of the ring, stabilizing each other for more than 100 mm. Afterwards the noise produced instability sets in and eventually breaks-up the structure, and two solitons are ejected. The dynamics of the composite structure break-up can be verified in Fig. 4.

Next, we investigate the energy exchange mechanism between the transversal field components for different values of the permittivity tensor ε_{zz} or, more appropriately, n_{zz}. The results are summarized in Fig. 5 and, as one can see, the effect of the longitudinal anisotropy on the energy transfer mechanism can be quite dramatic. In all cases the E_z component is omitted for the sake of clarity, but it can be easily obtained via Gauss' law as stated previously. It is noteworthy mentioning that the sudden drop of the intensity curves only indicates that the solitons have actually left the computational window. The arrows in these figures indicate the point where the rupture of the vortex becomes inevitable due to noise produced instability. Prior to the dipole-mode soliton break-up, there is a consistent energy transfer between the two induced channels, observed for all cases studied here. The reason for this to occur comes from the phase matching condition for the field in each induced channel. This phase matching condition is soon destroyed once a significant amount of energy is transferred from one channel to the other. Since the local refractive index depends strongly on the field intensity, each channel will produce a different local refractive index and, consequently, different local propagation constants. The result of this intensity unbalancing is the repulsion of the solitons, which fly off tangentially, as shown in Figs. 3 and 4.

The impact of the results shown in this work, particularly those in Fig. 5, can be quite significant if one is interested in designing practical optical devices with anisotropic CQ materials. Anisotropy, if properly controlled, can be a useful additional degree of freedom in the design of polarization sensitive structures, for instance. Even though we have not shown here results for 1% variation in n_{zz} (which was due only to the computational time required, since the propagation distance would be significantly longer), we strongly believe that a similar pattern would be observed.

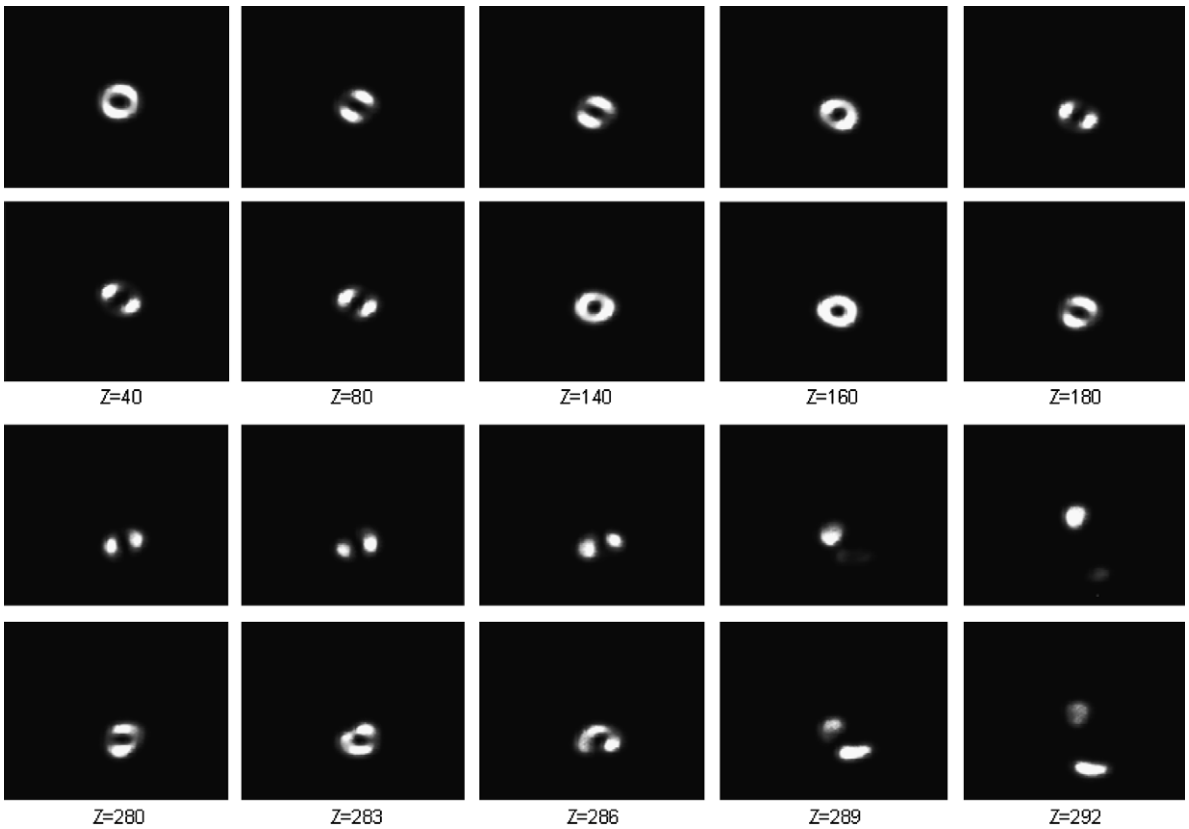

Fig. 3. Vortex propagation in an anisotropic CQ non-linear material, with $n_{xx} = n_{yy} = 2.5$ and $n_{zz} = 2.5 + \Delta$, where $\Delta = 0.05$ (2% variation). The upper and lower rows of each sequence represent the intensity distributions for the E_x and E_y components, respectively. The points were the fields were sampled are indicated in the figure (z is in mm).

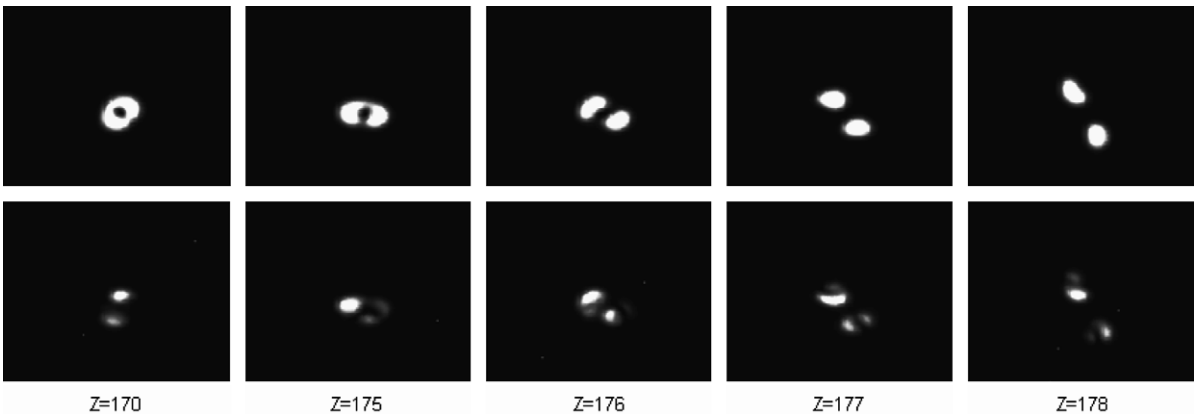

Fig. 4. Vortex propagation in an anisotropic CQ non-linear material, with $n_{xx} = n_{yy} = 2.5$ and $n_{zz} = 2.5 + \Delta$, where $\Delta = 0.125$ (5% variation). The upper and lower rows represent the intensity distribution for the E_x and E_y.

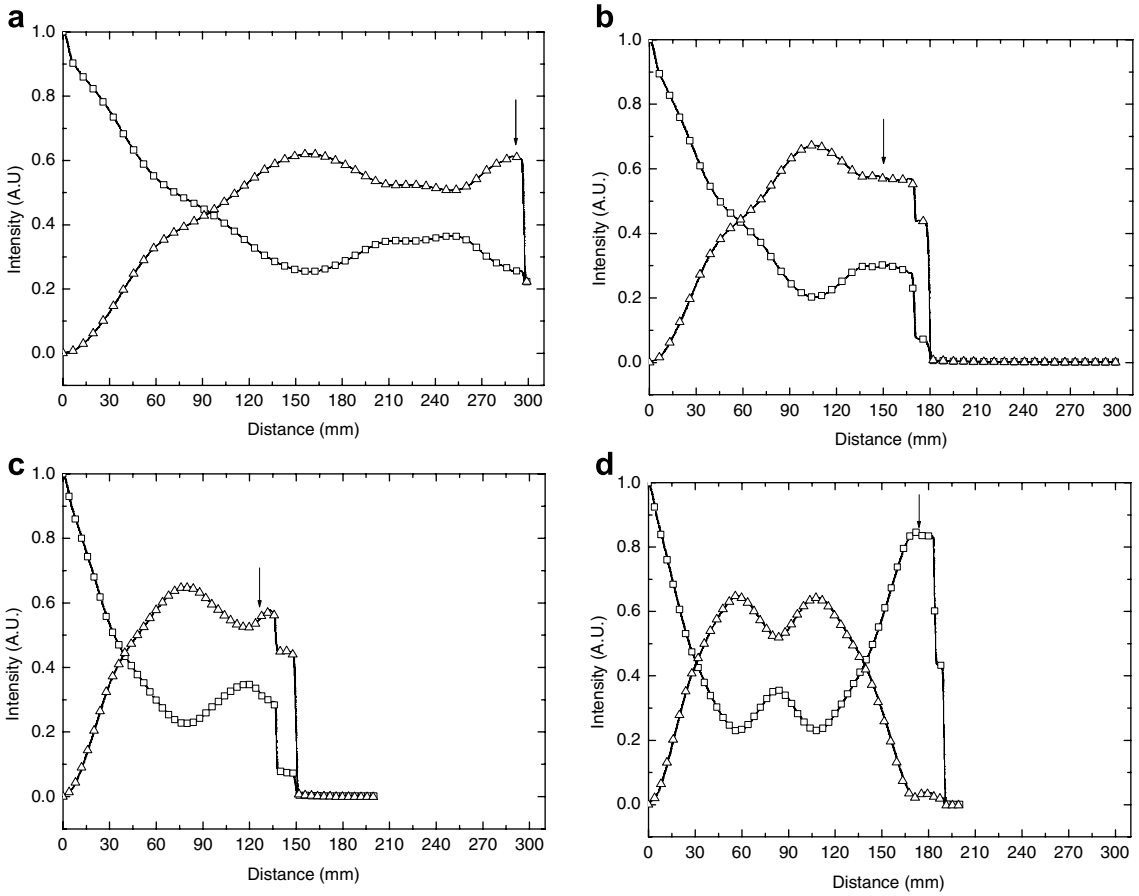

Fig. 5. Field intensity for the transverse components E_x (squares) and E_y (triangles), with $n_{xx} = n_{yy} = 2.5$, and $n_{zz} = 2.5 + \Delta$. (a) $\Delta = 0.05$, (b) $\Delta = 0.075$, (c) $\Delta = 0.1$, and (d) $\Delta = 0.125$. The arrows indicate the point where the rupture of the vortex begins to occur. The intensity drops to zero when the vortices leave the computational window.

The stationary behavior of the dipole-mode solitons (for tens of diffraction lengths) appears to be a good candidate structure for the design of reconfigurable waveguides, as suggested by [21].

This study also paves the way for the inclusion of an even more striking degree of freedom in the design of advanced structures, namely the magnetooptic effect. This effect, together with anisotropy, can be explored in the design of non-reciprocal devices, or as a trigger for the breaking-up of the vortex structure at a given point along the propagation. We expect to address these aspects in future publications.

4. Conclusion

This paper presented for the first time a full-vectorial analysis of optical vortex propagation in anisotropic cubic-quintic non-linear medium. The purpose was to investigate the energy transfer mechanism and the stability between orthogonal field components and how they are affected by the presence of anisotropy in this material. The numerical simulations were carried out by means of a three-dimensional finite difference based beam propagation method (3D-FD-BPM). In these simulations all elements of the permittivity tensor were allowed to vary (one at a time) so that the stability of vortex propagation could be verified. The anisotropic CQ non-linear media was insensitive to variations in the transverse tensor elements, namely n_{xx} and n_{yy}. The same was no longer true when the longitudinal component, n_{zz}, was varied. Therefore, we carried out a stability analysis by allowing n_{zz} to vary positively from 2% to 5% (we did not check for 1% variation due to the long computational time required, but we strongly believe the same behavior would still be observed). The effect on the vortex stability was dramatic, even for the lowest variation on n_{zz}. We observed that small variations in n_{zz}, besides contributing to the energy transfer between transversal field components, also caused the splitting of the vortex ring giving rise to a dipole-mode soliton which propagated in a stationary fashion for several diffraction lengths. The rupture of the dipole-mode eventually occurred and two solitons were then ejected tangentially.

Finally, we believe this work provided new and important information regarding the behavior of these objects that may prove to be quite useful for the design of new photonic devices.

Acknowledgements

This work was supported in part by the Brazilian agencies FAPESP (The State of São Paulo Research Foundation) and CNPq (The National Council for Scientific and Technological Development).

References

[1] J.F. Nye, M.V. Berry, Proc. R. Soc. Lond. A 336 (1974) 165.
[2] G.A. Swartzlander, D.R. Andersen, J.J. Regan, H. Yin, A. Kaplan, Phys. Rev. Lett. 66 (1991) 1583.
[3] A. Snyder, L. Poladian, D.J. Mitchel, Opt. Lett. 17 (1992) 789.
[4] B.A. Malomed, G.D. Peng, P.L. Chu, I. Towers, A.V. Buryak, R.A. Sammut, J. Pramana, Physics 57 (5–6) (2001) 1061.
[5] A.S. Desyatnikov, Yu. S. Kivshar, L. Torner, in: E. Wolf (Ed.), Progress in Optics, vol. 47, Elsevier, Amsterdam, 2005, p. 219.
[6] Y.S. Kivshar, B. Luther-Davies, Phys. Reports 298 (1998) 81.
[7] A.S. Desyatnikov, D. Mihalache, D. Mazilu, B.A. Malomed, C. Denz, F. Lederer, Phys. Rev. E 71 (2005) 026615.
[8] I. Towers, A.V. Buryak, R.A. Sammut, B.A. Malomed, Phys. Rev. E 63 (5) (2001) 055601 (R).
[9] M. Quiroga-Teixeiro, H. Michinel, J. Opt. Soc. Am. B 14 (8) (1997) 2004.
[10] D. Mihalache, Rom. J. Phys. 50 (3–4) (2005) 357.
[11] D. Mihalache, D. Mazilu, B.A. Malomed, F. Lederer, Phys. Rev. E 69 (2004) 066614.
[12] I. Towers, A.V. Buryak, R.A. Sammut, B.A. Malomed, L.-C. Crasovan, D. Mihalache, Phys. Lett. A 288 (2001) 292.
[13] B.A. Malomed, L.-C. Crasovan, D. Mihalache, Physica D 161 (2002) 187.
[14] D. Mihalache, D. Mazilu, I. Towers, B.A. Malomed, F. Lederer, J. Opt. A: Pure Appl. Opt. 4 (2002) 615.
[15] R.L. Pego, H.A. Warchall, J. Non-linear Sci. 12 (2002) 347.
[16] L.-C. Crasovan, B.A. Malomed, D. Mihalache, Phys. Rev. E 63 (2001) 016605.
[17] D. Mihalache, D. Mazilu, L.-C. Crasovan, I. Towers, B.A. Malomed, A.V. Buryak, L. Torner, F. Lederer, Phys. Rev. E 66 (2002) 016613.
[18] D. Mihalache, D. Mazilu, L.-C. Crasovan, I. Towers, A.V. Buryak, B.A. Malomed, L. Torner, J.P. Torres, F. Lederer, Phys. Rev. Lett. 88 (2002) 073902.
[19] D. Mihalache, D. Mazilu, F. Lederer, Y.V. Kartashov, L.-C. Crasovan, L. Torner, B.A. Malomed, Phys. Rev. Lett. 97 (2006) 073904.
[20] W. Krolikowski, E.A. Ostrovskaya, C. Weilnau, M. Geisser, G. McCarthy, Y.S. Kivshar, C. Denz, B. Luther-Davies, Phys. Ver. Lett. 85 (7) (2000) 1424.
[21] A.H. Carlsson, J.N. Malmberg, D. Anderson, M. Lisak, E.A. Ostrovskaya, T.J. Alexander, Y.S. Kivshar, Opt. Lett. 25 (9) (2000) 660.
[22] L.D.S. Alcantara, F.L. Teixeira, A.C. César, B.-H.V. Borges, J. Lightwave Technol. 23 (8) (2005) 2579.
[23] H. Michinel, J. Campo-Táboas, M.L. Quiroga-Teixeiro, J.R. Salgueiro, R. García-Fernández, J. Opt. B: Quantum Semiclass. Opt. 3 (2001) 314.
[24] M.J. Paz-Alonso, H. Michinel, Phys. Rev. Lett. 94 (2005) 093901.
[25] V.I. Mikla, V.M. Kryshenik, J. Non-Cryst. Solids 330 (2003) 33.
[26] V.M. Kryshenik, V.P. Ivanitsky, V.S. Kovtunenko, J.Optoelectron. Adv. Mater. 7 (6) (2005) 2953.
[27] Y.S. Kivshar, J. Christou, V. Tikhonenko, B. Luther-Davies, L.M. Pismen, Opt. Commun. 152 (1998) 198.
[28] K. Staliunas, Opt. Commun. 90 (1992) 123.
[29] D.V. Skryabin, Phys. Rev. A 63 (2000) 013602.
[30] B.A. Malomed, D. Mihalache, F. Wise, L. Torner, J. Opt. B: Quantum Semiclass. Opt. 7 (2005) R53.
[31] J.J. García-Ripoll, V.M. Pérez-García, E.A. Ostrovskaya, Y.S. Kivshar, Phys. Rev. Lett. 85 (1) (2000) 82.
[32] M.R. Belic, D. Vujic, A. Stepken, F. Kaiser, G.F. Calvo, F. Agulló-López, M. Carrascosa, Phys. Rev. E 65 (2002) 066610.
[33] M. Ahles, K. Motzek, A. Stepken, F. Kaiser, C. Weilnau, C. Denz, J. Opt. Soc. Am. B 19 (3) (2002) 557.